ECCOMAS Congress 2016
VII European Congress on Computational Methods in Applied Sciences and Engineering
M. Papadrakakis, V. Papadopoulos, G. Stefanou, V. Plevris (eds.)
Crete Island, Greece, 5–10 June 2016

A DEGENERATE-CONTINUUM BASED TIMOSHENKO BEAM APPROACH FOR THE AEROELASTIC ANALYSIS OF THE WIND TURBINE BLADES

Anthoula N. Panteli[1], **Dimitris I. Manolas**[2], **and Konstantinos V. Spiliopoulos**[1]

[1]School of Civil Engineering, Institute of Structural Analysis and Antiseismic Research,
National Technical University of Athens, Zografou Campus, 157-80 Athens, Greece
e-mail: {anpanteli, kvspilio} @central.ntua.gr

[2] School of Mechanical Engineering, Section of Fluids,
National Technical University of Athens, Zografou Campus, 157-80 Athens, Greece
e-mail: manolasd@fluid.mech.ntua.gr

Keywords: aeroelasticity, wind turbine blades, large displacements, finite rotations, geometrically non-linear effects, Total Lagrangian formulation

Abstract. *Due to the substantial increase of the size of current and future wind turbine designs, the blades tend to be quite flexible, resulting to large displacements and finite rotations under the action of the aerodynamic loading. As a result, the geometry of the blades changes, in some cases the flap deflection exceeds* 10% *of the blade radius, and thus, geometrically non-linear effects of significant importance take place.*
Two geometrically non-linear models are available in the multi-body hydro-servo-aeroelastic tool hGAST [1, 2], the first employs a 2nd order Euler-Bernoulli beam approach and the second is based on a non-linear sub-body modeling of the blades. In the present paper, a degenerate-continuum based Timoshenko beam approach is presented, which has been implemented in the code. The main kinematic assumptions are that the cross-section remains plane and rigid in its own plane, hence, the cross-sectional out-of-plane and in-plane warpings are neglected. The material is assumed homogeneous, isotropic, linear and elastic.
Comparisons between the non-linear models and the linear one are presented. The basic outcome from the analysis of a three-bladed rotor, with aerodynamic and structural properties same to the 5MW NREL reference wind turbine, is that the non-linear models result to a significant difference in torsional response compared to the linear model, due to the bending-torsion non-linear coupling. This could be an important aspect for the design of the blades, since it contributes to passive load reduction strategies.

1 INTRODUCTION

In bibliography, geometrically non-linear beam theories could be separated into two categories: a degenerate-continuum beam theory [3, 4, 5] and a geometrically exact beam theory [6, 7]. The first category, which has been inspired by the work done for shells (first introduced in 1968 by Ahmad et al. [8]), is directly derived from the 3D-continuum. The strain-displacement relations used are written in a strong sense, i.e. at the material particle level. The second category, which has been introduced by Reissner [6] for the plane case and by Simo [7] for the spatial case, deals with the problem formulation at a beam theory level. The strain-displacement relations used are written in a weak sense, i.e. at the reference point of the beam. These *generalized* strain measures do not spoil the geometric exactness, as this is expressed via the resultant form of the differential equilibrium equations at the deformed state. Actually, Reissner [9] had proposed a formulation in 3D before Simo, but, using a rotation matrix simplification to derive the required strain-displacement relations, he spoiled the geometric exactness [10]. Many finite-element developers of the beam theories, e.g. Jelenić & Crisfield [10], Cardona & Geradin [11], Ibrahimbegović [12], based their approach on the geometrically exact beam theory.

The more flexible wind turbine blades of modern design lead to a strong coupling between aerodynamics and structural dynamics, namely the aeroelasticity. Thus, the structural models used in aeroelasticity of the blades need to account for the exact geometry of the deformed shape, so that an accurate input for the aerodynamics load estimation may be provided. A review on the structural models used in aeroelasticity of the blades is given in [13]. As far as the 1D structural models are concerned, linear beam models had been used for long. Important terms which consider certain non-linearities were included, i.e. coupling-type terms associated with the centrifugal forces. Today, two non-linear beam theory models for rotor blades are used: One is the moderate deflection beam model [9, 14] based on ordering schemes, and, the other is the large deflection beam model [15, 16] developed according to the aforementioned geometrically exact beam theory.

As far as the aerodynamics is concerned, the aerodynamic model, used to transform the wind flow field to loads on the blades, is a (BEM) Blade-Element Momentum model, which accounts for dynamic inflow, yaw misalignment, and dynamic stall effects [17].

In this work, a Total Lagrangian beam approach based on the degenerate-continuum concept, for using it in aeroelasticity, is presented. The difference compared to the beam theory model presented in [3, 4, 5] is that before the element interpolation is performed, an analytical integration over the cross-section is carried out to reduce the 3D integration to a 1D integration. The same procedure is followed in [18] for an Updated Lagrangian formulation. The paper outline is as follows: In section 2, the kinematics and kinetics of the degenerate-continuum based beam formulation are presented. An important issue is how to represent the finite rotations of the cross-section. In the present work, the rotational vector representation technique is used to avoid the non-uniqueness problem associated to the Euler angles one [19]. The exponential mapping of the skew-symmetric matrix of the rotational vector is evaluated to update the cross-sectional orientation. Consistent linearization of the configuration state is presented in the following, needed to construct a step-by-step analysis, in the context of a Total Lagrangian formulation. In section 3, the linearized equilibrium equation is presented, from which the beam matrices are derived after the discretization procedure, using the finite element method. In section 4, the numerical results from the three-bladed 5MW NREL [20] rotor motion, under uniform inflow conditions, are presented. Comparisons are given between the three options of the geometrically non-linear modeling (degenerate-continuum based, 2nd order Euler-Bernoulli, sub-body

approach models) and the linear one.

2 DEGENERATE-CONTINUUM BASED TIMOSHENKO BEAM APPROACH

2.1 Assumptions

- The cross-section of the beam remains plane and rigid inside its own plane, hence, warping is not included. However, the warping displacement behavior could be added to the assumed deformations.
- Shear deformation is taken into account, and, it is assumed constant in the cross-section as a consequence of the previous non-warping assumption.
- The initial reference line of the beam is assumed, for the sake of simplicity, straight.
- The material is homogeneous, isotropic and linear elastic.

2.2 Basic kinematics

The reference bases used in kinematics are (fig. 1),

- $\boldsymbol{E_j}, j = 1 - 3$, is the orthonormal body-attached reference basis (which is rotating in the context of the blade dynamics)
- $\boldsymbol{V_i}(\xi), i = r, s, t$, is the orthonormal moving basis, attached to each cross-section

where, ξ is the arc-length variable along the reference line of the beam.

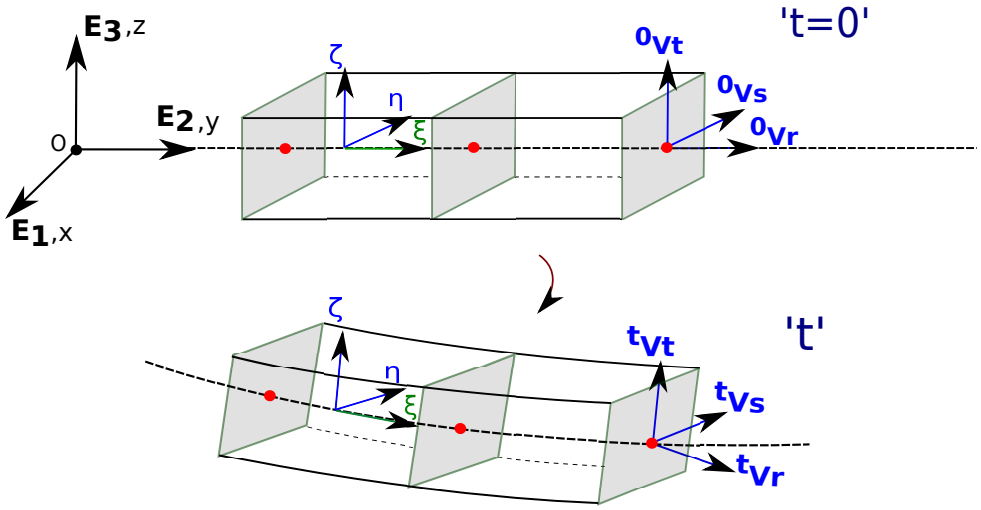

Fig. 1: Initial and deformed configuration of the beam.

2.2.1 Initial configuration state

The initial cross-sectional orientation is expressed via the initial orthogonal transformation $\xi \rightarrow {}^0\mathbf{\Lambda}(\xi) \in SO(3)$, $SO(3)$ is the special orthogonal group, thus, the moving frame basis at the initial (undeformed) state (fig. 1) is given by,

$$ {}^0\boldsymbol{V_i}(\xi) = {}^0\Lambda_{ij}(\xi)\boldsymbol{E_j} \tag{1}$$

The triads ${}^0\boldsymbol{V_i}(\xi), i = r, s, t$ are directed along the axes shown in fig. 1, which are parallel to the reference basis $\boldsymbol{E_j}, j = 1 - 3$, (in blade dynamics the origin of these triads is located on the pitch axis of the blade). The basis vectors ${}^0\boldsymbol{V_i}(\xi)$, in general, depend on ξ due to the presence of initial curvatures and/or twist. In the present, because of the straight beam assumption, these vectors are constant along the beam. The corresponding position vector $\boldsymbol{R}$ of an arbitrary material particle (ξ, η, ζ) of the undeformed beam is given by,

$$ \boldsymbol{R}(\xi, \eta, \zeta) = \boldsymbol{R_0}(\xi) + {}^0\mathbf{\Lambda^T} \cdot \begin{Bmatrix} 0 \\ \eta \\ \zeta \end{Bmatrix} = \boldsymbol{R_0}(\xi) + \eta \cdot {}^0\boldsymbol{V_s} + \zeta \cdot {}^0\boldsymbol{V_t} \tag{2}$$

where, $\boldsymbol{R_0}(\xi)$ is the position vector of the undeformed beam reference point.

2.2.2 Current configuration state

In a similar way, the deformed cross-sectional orientation is expressed via the orthogonal transformation $\xi \rightarrow {}^t\mathbf{\Lambda}(\xi) \in SO(3)$, thus, the moving frame basis at the current (deformed) state (fig. 1) is given by,

$$ {}^t\boldsymbol{V_i}(\xi) = {}^t\Lambda_{ij}(\xi)\boldsymbol{E_j} \tag{3}$$

The Bernoulli hypothesis of the plane cross-sections remaining planar after deformation and retaining their shape and area is assumed to hold, thus, the corresponding position vector ${}^t\boldsymbol{r}$ of an arbitrary material particle (ξ, η, ζ) of the deformed beam is given by,

$$ {}^t\boldsymbol{r}(\xi, \eta, \zeta) = {}^t\boldsymbol{r_0}(\xi) + {}^t\mathbf{\Lambda^T}(\xi) \cdot \begin{Bmatrix} 0 \\ \eta \\ \zeta \end{Bmatrix} = {}^t\boldsymbol{r_0}(\xi) + \eta \cdot {}^t\boldsymbol{V_s}(\xi) + \zeta \cdot {}^t\boldsymbol{V_t}(\xi) \tag{4}$$

where, ${}^t\boldsymbol{r_0}(\xi)$ is the position vector of the deformed beam reference point.

2.3 Updated (trial) configuration state

The update of the configuration state w.r.t. the displacements is conventional, i.e. additive, due to their vectorial nature. To update the configuration state w.r.t. the rotations, the cross-sectional orientation at configurations $t + \Delta t$ and t are related via the rotational (pseudo)-vector $\boldsymbol{\theta}(\xi)$ (fig. 2), which rotates the base vectors ${}^t\boldsymbol{V_i}(\xi)$ into the base vectors ${}^{t+\Delta t}\boldsymbol{V_i}(\xi)$ around the axis $\frac{1}{\theta(\xi)} \cdot \boldsymbol{\theta}(\xi)$ for the angle $\theta(\xi)$, through

$$ {}^{t+\Delta t}\boldsymbol{V_i}(\xi) = \mathbf{\Lambda}(\xi)\ {}^t\boldsymbol{V_i}(\xi) = exp(\hat{\boldsymbol{\theta}}(\xi))\ {}^t\boldsymbol{V_i}(\xi), \quad i = r, s, t \tag{5}$$

where, the rotation matrix $\mathbf{\Lambda}(\xi)$ is given by,

$$ \mathbf{\Lambda}(\xi) = exp(\hat{\boldsymbol{\theta}}(\xi)) = \boldsymbol{I} + \frac{sin\theta}{\theta}\hat{\boldsymbol{\theta}} + \frac{1 - cos\theta}{\theta^2}\hat{\boldsymbol{\theta}}\hat{\boldsymbol{\theta}} \tag{6}$$

where $\hat{\boldsymbol{\theta}}(\xi)$ is the skew-symmetric matrix formed by the components of the rotational vector $\boldsymbol{\theta}(\xi)$ ($\hat{\boldsymbol{\theta}}(\xi) = -e^{ij}_k \theta^k \boldsymbol{E_i} \boldsymbol{E_j^T}$; e^{ij}_k is the permutation symbol). The above formula is the well-known Rodrigues formula. Details about the derivation of the formula one could find at [3, 21].

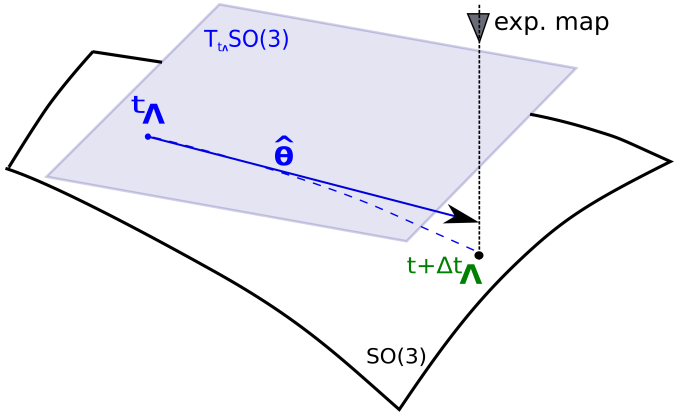

Fig. 2: Geometric interpretation of the exponential map, $T_{{}^t\Lambda}SO(3)$: tangent plane at ${}^t\boldsymbol{\Lambda}$ [22].

2.3.1 Strain and stress measures at the updated (trial) configuration state

By subtracting the position vector at $t = 0$, given in eq. (2), from the position vector at $t + \Delta t$, given in eq. (4) for $t = t + \Delta t$, for an arbitrary material particle (ξ, η, ζ) of the beam, the displacement field at $t + \Delta t$ is written as follows,

$$ {}^{t+\Delta t}\boldsymbol{u}(\xi,\eta,\zeta) = {}^{t+\Delta t}\boldsymbol{u}_0(\xi) + \eta \cdot {}^{t+\Delta t}\boldsymbol{\Delta V_s}(\xi) + \zeta \cdot {}^{t+\Delta t}\boldsymbol{\Delta V_t}(\xi) \tag{7} $$

where, ${}^{t+\Delta t}\boldsymbol{u}_0(\xi)$ is the updated displacement of the beam reference point, and, ${}^{t+\Delta t}\boldsymbol{\Delta V_s}(\xi)$, ${}^{t+\Delta t}\boldsymbol{\Delta V_t}(\xi)$ are the differences between the initial and the updated cross-sectional directors.

To know the stress condition contributing to the geometric stiffness in the context of the Newton-Raphson iterative procedure, the internal forces and moments of the beam at the trial state $t + \Delta t$ need to be evaluated. To do so, the steps below are followed (for convenience, the variables ξ, η, ζ are omitted from the RHS),

1. The material particle (ξ, η, ζ) global displacement gradients are evaluated,

$$ \left\{ {}^{t+\Delta t}u_{,x}\ {}^{t+\Delta t}u_{,y}\ {}^{t+\Delta t}u_{,z}\ {}^{t+\Delta t}v_{,x}\ {}^{t+\Delta t}v_{,y}\ {}^{t+\Delta t}v_{,z}\ {}^{t+\Delta t}w_{,x}\ {}^{t+\Delta t}w_{,y}\ {}^{t+\Delta t}w_{,z} \right\}^T $$

   where, ${}^{t+\Delta t}u$, ${}^{t+\Delta t}v$, ${}^{t+\Delta t}w$ are the components of the updated displacement (eq. 7) w.r.t. the reference basis $\boldsymbol{E}$, while, (,) denotes the spatial derivative relative to the x, y, z coordinates.

2. Using the coordinate transformation of a 2nd order tensor [23], the global displacement gradients are rotated to get the initial local ones, i.e. relative to the initial cross-sectional basis ${}^0\boldsymbol{V}$.

3. The components of the Green strain tensor [3, 4] are evaluated. Because of the assumption that the cross-sectional shape does not change during deformation, the only remaining

components of the Green strain tensor are,

$$
\begin{aligned}
{}^{t+\Delta t}\epsilon_{\xi\xi}(\xi,\eta,\zeta) &= {}^{t+\Delta t}u_{\xi,\xi} + \frac{1}{2}({}^{t+\Delta t}u_{\xi,\xi})^2 + \frac{1}{2}({}^{t+\Delta t}v_{\eta,\xi})^2 + \frac{1}{2}({}^{t+\Delta t}w_{\zeta,\xi})^2 \\
{}^{t+\Delta t}\epsilon_{\xi\eta}(\xi,\eta,\zeta) &= \frac{1}{2}({}^{t+\Delta t}u_{\xi,\eta} + {}^{t+\Delta t}v_{\eta,\xi} + {}^{t+\Delta t}u_{\xi,\xi}{}^{t+\Delta t}u_{\xi,\eta} + {}^{t+\Delta t}v_{\eta,\xi}{}^{t+\Delta t}v_{\eta,\eta} \\
&\qquad + {}^{t+\Delta t}w_{\zeta,\xi}{}^{t+\Delta t}w_{\zeta,\eta}) \\
{}^{t+\Delta t}\epsilon_{\xi\zeta}(\xi,\eta,\zeta) &= \frac{1}{2}({}^{t+\Delta t}u_{\xi,\zeta} + {}^{t+\Delta t}w_{\zeta,\xi} + {}^{t+\Delta t}u_{\xi,\xi}{}^{t+\Delta t}u_{\xi,\zeta} + {}^{t+\Delta t}v_{\eta,\xi}{}^{t+\Delta t}v_{\eta,\zeta} \\
&\qquad + {}^{t+\Delta t}w_{\zeta,\xi}{}^{t+\Delta t}w_{\zeta,\zeta}) \qquad (8)
\end{aligned}
$$

where, ${}^{t+\Delta t}u_{\xi}, {}^{t+\Delta t}v_{\eta}, {}^{t+\Delta t}w_{\zeta}$ are the updated displacements of an arbitrary material particle w.r.t. the cross-sectional basis ${}^{\mathbf{0}}\boldsymbol{V}$, while, (,) denotes the spatial derivative relative to the ξ, η, ζ coordinates.

4. The internal forces/moments that arise in the geometric stiffness due to the 2nd Piola-Kirchhoff normal stress ${}^{t+\Delta t}S_{\xi\xi}(\xi,\eta,\zeta)$ are defined as,

$$
\begin{aligned}
{}^{t+\Delta t}F_{\xi\xi}(\xi) &= \int_{{}^0A} {}^{t+\Delta t}S_{\xi\xi}\, d^0A, & {}^{t+\Delta t}M_{\eta\eta}(\xi) &= \int_{{}^0A} \zeta \cdot {}^{t+\Delta t}S_{\xi\xi}\, d^0A \\
{}^{t+\Delta t}M_{\zeta\zeta}(\xi) &= \int_{{}^0A} \eta \cdot {}^{t+\Delta t}S_{\xi\xi}\, d^0A, & {}^{t+\Delta t}M_{\xi\xi 1}(\xi) &= \int_{{}^0A} \eta^2 \cdot {}^{t+\Delta t}S_{\xi\xi}\, d^0A \\
{}^{t+\Delta t}M_{\xi\xi 2}(\xi) &= \int_{{}^0A} \zeta^2 \cdot {}^{t+\Delta t}S_{\xi\xi}\, d^0A, & {}^{t+\Delta t}M_{\xi\xi 3}(\xi) &= \int_{{}^0A} \eta\zeta \cdot {}^{t+\Delta t}S_{\xi\xi}\, d^0A \qquad (9)
\end{aligned}
$$

where, ${}^0A$ is the initial cross-sectional area, ${}^{t+\Delta t}S_{\xi\xi}(\xi,\eta,\zeta) = E \cdot {}^{t+\Delta t}\epsilon_{\xi\xi}$, E is the Young's modulus, ${}^{t+\Delta t}F_{\xi\xi}(\xi)$ is the normal force, ${}^{t+\Delta t}M_{\eta\eta}(\xi)$, ${}^{t+\Delta t}M_{\zeta\zeta}(\xi)$ are the bending moments, and, ${}^{t+\Delta t}M_{\xi\xi 1-3}(\xi)$ lead to the effective torsional moment components due to the bending, all referred to the initial state. A geometrical interpretation of the last internal moment is given in [24].
The internal forces/moments that arise in the geometric stiffness due to the 2nd Piola-Kirchhoff shear stress ${}^{t+\Delta t}S_{\xi\eta}(\xi,\eta,\zeta), {}^{t+\Delta t}S_{\xi\zeta}(\xi,\eta,\zeta)$ are defined as,

$$
\begin{aligned}
{}^{t+\Delta t}F_{\xi\eta}(\xi) &= \int_{{}^0A} {}^{t+\Delta t}S_{\xi\eta}\, d^0A, & {}^{t+\Delta t}F_{\xi\zeta}(\xi) &= \int_{{}^0A} {}^{t+\Delta t}S_{\xi\zeta}\, d^0A \\
{}^{t+\Delta t}M_{\xi\xi 4}(\xi) &= \int_{{}^0A} \zeta \cdot {}^{t+\Delta t}S_{\xi\eta}\, d^0A, & {}^{t+\Delta t}M_{\xi\xi 5}(\xi) &= \int_{{}^0A} \eta \cdot {}^{t+\Delta t}S_{\xi\zeta}\, d^0A \qquad (10)
\end{aligned}
$$

where, ${}^{t+\Delta t}S_{\xi\eta}(\xi,\eta,\zeta) = G \cdot (2^{t+\Delta t}\epsilon_{\xi\eta})$, ${}^{t+\Delta t}S_{\xi\zeta}(\xi,\eta,\zeta) = G \cdot (2^{t+\Delta t}\epsilon_{\xi\zeta})$, G is the shear modulus, ${}^{t+\Delta t}F_{\xi\eta}(\xi)$, ${}^{t+\Delta t}F_{\xi\zeta}(\xi)$ are the shear forces, and, ${}^{t+\Delta t}M_{\xi\xi 4-5}(\xi)$ lead to the torsional moment components, all referred to the initial state.

By performing the cross-sectional integration analytically, the internal forces and moments are derived in relation with the cross-sectional properties and a resultant form of the strain measures.

Remark: At the updated configuration $t + \Delta t$,

- *'Rotations'* contribute in the internal elastic energy are depicted in the difference

$$
{}^{t+\Delta t}\boldsymbol{\Delta V_i}(\xi) = {}^{t+\Delta t}\boldsymbol{V_i}(\xi) - {}^0\boldsymbol{V_i}, i = s, t \qquad (11)
$$

- *'Curvature' measures* contribute in the internal elastic energy are depicted in the derivative of the above difference along the beam arc-length, $\frac{\vartheta^{t+\Delta t}\boldsymbol{\Delta V_i}(\xi)}{\vartheta\xi}, i = s, t$:

$$\frac{\vartheta({}^{t+\Delta t}\boldsymbol{V_i}(\xi) - {}^{0}\boldsymbol{V_i})}{\vartheta\xi} = \frac{\vartheta(exp(\hat{\boldsymbol{\theta}}(\xi))\,{}^{t}\boldsymbol{V_i}(\xi))}{\vartheta\xi} \tag{12}$$

where the orientation update relation (5) has been used.

For the differentiation of the exponential mapping we refer to [25], where a family of trigonometric functions, that have been used, facilitate the procedure significantly.

2.4 Perturbation of the configuration state at $t + \Delta t$

To construct the perturbed configuration state at $t + \Delta t$,

- The perturbed position of the reference line relative to ${}^{t+\Delta t}\boldsymbol{r_0}(\xi)$ is constructed as,

$${}^{t+\Delta t,\epsilon}\boldsymbol{r_0}(\xi) = {}^{t+\Delta t}\boldsymbol{r_0}(\xi) + \epsilon\,\delta\boldsymbol{u_0}(\xi) \tag{13}$$

where, $\delta\boldsymbol{u_0}(\xi) = \delta u_{0i}(\xi)\boldsymbol{E_i}$ is a vector field, interpreted, for $\epsilon > 0$, as superposed infinitesimal displacement onto the reference line [22].

- The perturbed orthogonal transformation relative to ${}^{t+\Delta t}\boldsymbol{\Lambda}(\xi)$, which consists of the cross-sectional basis ${}^{t+\Delta t}\boldsymbol{V}(\xi)$ as given in eq. (5), is constructed by two ways (fig. 3),

a)

$${}^{t+\Delta t,\epsilon}\boldsymbol{\Lambda}(\xi) = exp(\epsilon\boldsymbol{\delta\Psi}(\xi))^{t+\Delta t}\boldsymbol{\Lambda}(\xi) = exp(\epsilon\boldsymbol{\delta\Psi}(\xi))exp(\hat{\boldsymbol{\theta}}(\xi))\,{}^{t}\boldsymbol{\Lambda}(\xi) \tag{14}$$

where, $\boldsymbol{\delta\Psi}(\xi)$ is a skew-symmetric tensor field, interpreted, for $\epsilon > 0$, as superposed infinitesimal rotation (spin) onto the moving frame [22]. The eq. (5) has been used above, in the form ${}^{t+\Delta t}\boldsymbol{\Lambda}(\xi) = exp(\hat{\boldsymbol{\theta}}(\xi))\,{}^{t}\boldsymbol{\Lambda}(\xi)$.

b)

$${}^{t+\Delta t,\epsilon}\boldsymbol{\Lambda}(\xi) = exp(\hat{\boldsymbol{\theta}}(\xi) + \epsilon\delta\hat{\boldsymbol{\theta}}(\xi))\,{}^{t}\boldsymbol{\Lambda}(\xi) \tag{15}$$

where, $\delta\hat{\boldsymbol{\theta}}(\xi)$ is a skew-symmetric tensor field, interpreted, for $\epsilon > 0$, as infinitesimal rotation that can be added to the previous rotation.

To get a relation between the axial vectors $\boldsymbol{\delta\psi}(\xi)$ and $\delta\boldsymbol{\theta}(\xi)$ of the skew-symmetric matrices $\boldsymbol{\delta\Psi}(\xi)$ and $\delta\hat{\boldsymbol{\theta}}(\xi)$ respectively, the Rodrigues formula is used in eqs. (14, 15) and then, the derivative with respect to the scalar parameter ϵ is taken, for $\epsilon = 0$ [26],

$$\boldsymbol{\delta\psi}(\xi) = \boldsymbol{T(\theta)}\delta\boldsymbol{\theta}(\xi) \tag{16}$$

where,

$$\boldsymbol{T(\theta)} = \frac{sin\theta}{\theta}\boldsymbol{I} + \frac{1 - cos\theta}{\theta^2}\hat{\boldsymbol{\theta}} + \frac{\theta - sin\theta}{\theta^3}\boldsymbol{\theta}\otimes\boldsymbol{\theta} \tag{17}$$

For the derivation of the transformation $\boldsymbol{T(\theta)}$ (named as the tangential transformation because is a linear map between tangent spaces, fig. 3) see [3, 11, 27].

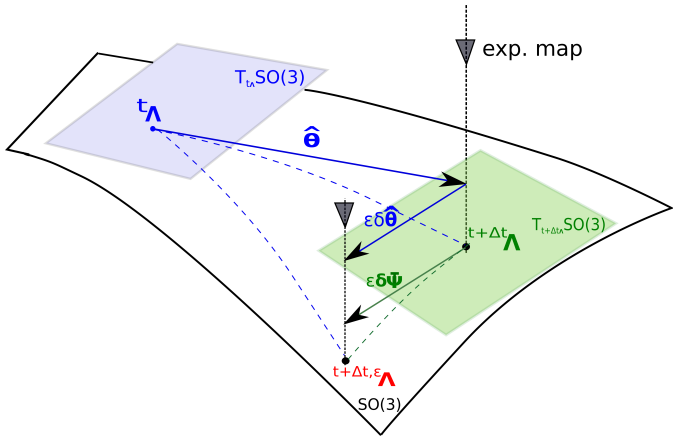

Fig. 3: Rotation increments and their projection onto the manifold SO(3) [11, 26].

2.4.1 Virtual strain measures

By employing the directional derivative onto the perturbed configuration state (eqs. 13, 14), the variation of the configuration state $(\delta \boldsymbol{r_0}(\xi), \delta \boldsymbol{\Lambda}(\xi))$ is derived,

$$\delta \boldsymbol{r_0}(\xi) = \frac{d}{d\epsilon}\bigg|_{\epsilon=0} {}^{t+\Delta t,\epsilon}\boldsymbol{r_0}(\xi) = \delta \boldsymbol{u_0}(\xi) \tag{18}$$

$$\delta \boldsymbol{\Lambda}(\xi) = \frac{d}{d\epsilon}\bigg|_{\epsilon=0} {}^{t+\Delta t,\epsilon}\boldsymbol{\Lambda}(\xi) = \boldsymbol{\delta\Psi}(\xi)\, {}^{t+\Delta t}\boldsymbol{\Lambda}(\xi) \tag{19}$$

Thus, the virtual displacement for an arbitrary material particle (ξ, η, ζ) is written as,

$$\delta \boldsymbol{u}(\xi,\eta,\zeta) = \delta \boldsymbol{u_0}(\xi) + \eta \cdot \delta \boldsymbol{V_s}(\xi) + \zeta \cdot \delta \boldsymbol{V_t}(\xi) \tag{20}$$

where, $\delta \boldsymbol{u_0}(\xi)$ is the virtual displacement of the beam reference point and $\delta \boldsymbol{V_i}(\xi) = \delta \boldsymbol{\Lambda_{ij}}(\xi)\boldsymbol{E_j}$, $i = r, s, t, j = 1-3$. Specifically, by using eqs. (16, 17, 19), the virtual cross-sectional directors are given as follows,

$$\delta \boldsymbol{V_s}(\xi) = \boldsymbol{\delta\Psi}(\xi)^{t+\Delta t}\boldsymbol{V_s}(\xi) = \boldsymbol{\delta\psi}(\xi) \times {}^{t+\Delta t}\boldsymbol{V_s}(\xi) = (\boldsymbol{T(\theta)}\delta\boldsymbol{\theta}(\xi)) \times {}^{t+\Delta t}\boldsymbol{V_s}(\xi) \tag{21}$$

$$\delta \boldsymbol{V_t}(\xi) = \boldsymbol{\delta\Psi}(\xi)^{t+\Delta t}\boldsymbol{V_t}(\xi) = \boldsymbol{\delta\psi}(\xi) \times {}^{t+\Delta t}\boldsymbol{V_t}(\xi) = (\boldsymbol{T(\theta)}\delta\boldsymbol{\theta}(\xi)) \times {}^{t+\Delta t}\boldsymbol{V_t}(\xi) \tag{22}$$

By substituting eq. (21) and eq. (22) in eq. (20), the material particle virtual displacement is written in relation with the unknown variables $\delta \boldsymbol{u_0}(\xi)$ and $\delta\boldsymbol{\theta}(\xi)$. The steps (1) and (2) from the section 2.3.1 are followed to get the initial local infinitesimal displacement gradients. Following [4] for a Total Lagrangian formulation, the corresponding components of Green-Lagrange strain tensor are given by,

- The linear virtual strain components are (for convenience the variables ξ, η, ζ are omitted from the RHS),

$$\begin{aligned}
\delta e_{\xi\xi}(\xi,\eta,\zeta) &= \delta u_{\xi,\xi} + {}^{t+\Delta t}u_{\xi,\xi}\,\delta u_{\xi,\xi} + {}^{t+\Delta t}v_{\eta,\xi}\,\delta v_{\eta,\xi} + {}^{t+\Delta t}w_{\zeta,\xi}\,\delta w_{\zeta,\xi} \\
\delta e_{\xi\eta}(\xi,\eta,\zeta) &= \frac{1}{2}(\delta u_{\xi,\eta} + \delta v_{\eta,\xi} + {}^{t+\Delta t}u_{\xi,\xi}\,\delta u_{\xi,\eta} + {}^{t+\Delta t}v_{\eta,\xi}\,\delta v_{\eta,\eta} + {}^{t+\Delta t}w_{\zeta,\xi}\,\delta w_{\zeta,\eta} \\
&\quad + {}^{t+\Delta t}u_{\xi,\eta}\delta u_{\xi,\xi} + {}^{t+\Delta t}v_{\eta,\eta}\,\delta v_{\eta,\xi} + {}^{t+\Delta t}w_{\zeta,\eta}\,\delta w_{\zeta,\xi}) \\
\delta e_{\xi\zeta}(\xi,\eta,\zeta) &= \frac{1}{2}(\delta u_{\xi,\zeta} + \delta w_{\zeta,\xi} + {}^{t+\Delta t}u_{\xi,\xi}\,\delta u_{\xi,\zeta} + {}^{t+\Delta t}v_{\eta,\xi}\,\delta v_{\eta,\zeta} + {}^{t+\Delta t}w_{\zeta,\xi}\,\delta w_{\zeta,\zeta} \\
&\quad + {}^{t+\Delta t}u_{\xi,\zeta}\,\delta u_{\xi,\xi} + {}^{t+\Delta t}v_{\eta,\zeta}\,\delta v_{\eta,\xi} + {}^{t+\Delta t}w_{\zeta,\zeta}\,\delta w_{\zeta,\xi})
\end{aligned} \tag{23}$$

where, $\delta u_\xi, \delta v_\eta, \delta w_\zeta$ are the components of the virtual displacement for the material particle (ξ, η, ζ), eq. (20), rotated to the cross-sectional basis ${}^{\mathbf{0}}\boldsymbol{V}$, and, (,) denotes the spatial derivative relative to the ξ, η, ζ coordinates.

- The non-linear virtual strain components are (for convenience the variables ξ, η, ζ are omitted from the RHS),

$$\begin{aligned}
\delta\eta_{\xi\xi}(\xi,\eta,\zeta) &= \frac{1}{2}(\delta u_{\xi,\xi}^2 + \delta v_{\eta,\xi}^2 + \delta w_{\zeta,\xi}^2) \\
\delta\eta_{\xi\eta}(\xi,\eta,\zeta) &= \frac{1}{2}(\delta u_{\xi,\xi}\delta u_{\xi,\eta} + \delta v_{\eta,\xi}\delta v_{\eta,\eta} + \delta w_{\zeta,\xi}\delta w_{\zeta,\eta}) \\
\delta\eta_{\xi\zeta}(\xi,\eta,\zeta) &= \frac{1}{2}(\delta u_{\xi,\xi}\delta u_{\xi,\zeta} + \delta v_{\eta,\xi}\delta v_{\eta,\zeta} + \delta w_{\zeta,\xi}\delta w_{\zeta,\zeta})
\end{aligned} \tag{24}$$

3 VIRTUAL WORK EQUATION FOR A TOTAL LAGRANGIAN FORMULATION

The equilibrium equation of the body at $(t + \Delta t, \epsilon)$ is given by [4],

$$\int_{{}^0V} {}^0\rho\, {}^{t+\Delta t,\epsilon}\ddot{r}_{Gk}\, \delta u_k d^0V + \int_{{}^0V} {}^{t+\Delta t,\epsilon}S_{ij}\, \delta^{t+\Delta t,\epsilon}\epsilon_{ij}\, d^0V = \int_{{}^0V} {}^{t+\Delta t}f_k^G\, \delta u_k\, d^0V + \int_{{}^{t+\Delta t}S_f} {}^{t+\Delta t}f_k^S\, \delta u_k^S\, d^{t+\Delta t}S \tag{25}$$

where, ${}^0V$ is the initial volume, ${}^0\rho$ is the mass density referred to the initial state, ${}^{t+\Delta t,\epsilon}\ddot{r}_{Gk}$, $k = \xi, \eta, \zeta$ is the acceleration of the particle due to all the inertia effects [2], i.e. the acceleration of the body origin, the Coriolis acceleration, and, the acceleration due to the body deformation, $\delta u_k = \left\{\delta u_\xi, \delta v_\eta, \delta w_\zeta\right\}^T$ are the virtual displacements, ${}^{t+\Delta t,\epsilon}S_{ij}$, $i, j = \xi, \eta, \zeta$, are the 2nd Piola-Kirchhoff stress components, $\delta^{t+\Delta t,\epsilon}\epsilon_{ij}$ are the virtual strains, ${}^{t+\Delta t}f_k^G$ is the gravitational load and ${}^{t+\Delta t}f_k^S$ is the surface aerodynamic load, where ${}^{t+\Delta t}S_f$ corresponds to the last calculated surface area.

For the linearization of the internal virtual work (2nd term of the LHS of the above relation 25), the iterative decompositions for stresses and strains are used,

$${}^{t+\Delta t,\epsilon}S_{ij} = {}^{t+\Delta t}S_{ij} + dS_{ij} \tag{26}$$

$${}^{t+\Delta t,\epsilon}\epsilon_{ij} = {}^{t+\Delta t}\epsilon_{ij} + d\epsilon_{ij},\ d\epsilon_{ij} = de_{ij} + d\eta_{ij} \tag{27}$$

where, ${}^{t+\Delta t}S_{ij} = C_{ijrs}\,{}^{t+\Delta t}\epsilon_{ij}$, C_{ijrs} expresses the material constitutive behaviour, ${}^{t+\Delta t}\epsilon_{ij}$ are given by eq. (8), $dS_{ij} = C_{ijrs}\, d\epsilon_{ij}$, de_{ij} is the linear strain part, given by the same relations as the corresponding virtual strain components (eqs. 23), and $d\eta_{ij}$ is the non-linear strain part, the variation of which is related to the geometrical stiffness. While variation and linearization can commute, the variation $\delta d\eta_{ij}$ is given by the chain-differentiation of eqs. (24).

Substituting in relation (25) the iterative decompositions (26) and (27), and following the

linearization process as it is presented in [4], the linearized equilibrium equation is derived,

$$\int_{{}^0V} {}^0\rho\, {}^{t+\Delta t,\epsilon}\ddot{r}_{Gk}\, \delta u_k d^0V + \left\{ \underbrace{\int_{{}^0V} C_{ijrs}\, de_{rs}\, \delta e_{ij}\, d^0V}_{\Rightarrow \boldsymbol{K_{mat}}} + \underbrace{\int_{{}^0V} {}^{t+\Delta t}S_{ij}\, \delta d\eta_{ij}\, d^0V}_{\Rightarrow \boldsymbol{K_{geom}}} \right\} =$$

$$\int_{{}^0V} {}^{t+\Delta t}f_k^G\, \delta u_k\, d^0V + \int_{{}^{t+\Delta t}S_f} {}^{t+\Delta t}f_k^S\, \delta u_k^S\, d^{t+\Delta t}S - \left(\underbrace{\int_{{}^0V} {}^{t+\Delta t}S_{ij}\, \delta e_{ij} d^0V}_{\Rightarrow \boldsymbol{F_{int}}} \right) \tag{28}$$

To construct the under-braced integrals, one has to substitute the strain components de_{rs}, δe_{ij} and $\delta d\eta_{ij}$ in eq. (28). By performing analytical integration over the cross-sectional area, the 1D form of the linearized virtual work is derived. After discretization, the matrices $\boldsymbol{K_{mat}}$, $\boldsymbol{K_{geom}}$ and the vector $\boldsymbol{F_{int}}$ are constructed. The first matrix refers to the resistance due to the linear constitutive behaviour of the material, while, the second one refers to the resistance due to the non-linear geometrical stiffness.

As far as the numerical implementation is concerned, one has to note two issues. The first is that the developed finite element is based on a quadratic interpolation, using a 2nd order Lagrange polynomial, of both the displacement and the rotation parameters, while, the second is that the mass matrix is evaluated using the initial configuration of the body, and thus, it is calculated prior to the step-by-step solution. Time integration is performed using the Newmark 2nd order implicit method [4].

4 NUMERICAL RESULTS

Time domain non-linear aeroelastic simulations for the isolated rotor of the 5MW NREL reference wind turbine [20] are performed, using the multi-body hydro-servo-aeroelastic tool hGAST [1, 2]. The present non-linear Degenerate-Continuum based Timoshenko beam model (non-linear DC) is compared to the 2nd order Euler-Bernoulli beam model (non-linear EB), the sub-body beam model (non-linear SB) and the linear one (linear). The transverse shear effect was neglected in view of enabling direct comparison with the 2nd order Euler-Bernoulli model. The 2nd order Euler-Bernoulli beam model accounts for moderate deflections by using an ordering scheme acted on the cross-sectional rotations [14, 28]. The sub-body modeling is an extension of the multi-body formulation to the body level. It consists of dividing the body (blade) into sub-bodies, which are subsequently treated as beam elements. At the sub-body level, local deflections and rotations are assumed small, and thus, the use of a linear Timoshenko beam model is justified, while by imposing kinematic and dynamic continuity between consecutive sub-bodies at their connection points, large deflections and rotations are gradually built [28]. The linear model accounts for the non-linear tension-bending coupling effect, which is added in the analysis of rotating bodies, since the centrifugal force increases their bending stiffness.

Uniform inflow conditions are considered at the rated wind speed of $11.4m/s$, where the deflections are expected to attain their maximum value and, in turn, the non-linear effects will be more pronounced. The rotor is operated at fixed rotational speed of $12rpm$ and at zero pitch angle (open loop operation, i.e. the controller is not active), corresponding to average operating conditions at the rated wind speed. The results are presented in terms of time histories, after the initial transients are damped.

In fig. 4, the blade tip twist angle is presented. The three non-linear models (non-linear DC, non-linear EB, non-linear SB) predict higher amplitudes of the twist angle variation as compared with the linear model. This is linked to the bending-torsion coupling effect [28] which is predicted only by the non-linear models. Although the twist angle amplitude as predicted by the non-linear SB model is $\sim 20\%$ reduced compared to the other two non-linear models, the phase of the signal is in perfect agreement between the three of them. Moreover, the non-linear models result to an increase of the twist angle mean value ($\sim 0.4^o$ for the non-linear SB model and $\sim 0.25^o$ for the other two non-linear models) compared to the linear model ($\sim 0.1^o$).

The increase in the amplitude of the twist angle affects the flapwise deflection (fig. 5) through the corresponding change in the effective angle of attack. So, in fig. 5, the three non-linear models depict a phase shift of the flapwise deflection signal compared to the linear model, following the phase of the torsion angle. Moreover, the non-linear DC and non-linear EB models predict the same amplitude of the flapwise deflection variation, although the non-linear DC model results to a slightly reduced mean value compared to the non-linear EB model. The non-linear SB model shows reduced amplitude of the variation ($\sim 25\%$) compared to the other two non-linear models, and slightly reduced compared to the linear model. The flapwise deflection mean value predicted by the non-linear SB model is identical to this of the linear modeling.

In fig. 6, the blade tip edgewise deflections are presented. As expected, the agreement between the four models is good, since the edgewise direction of the blade is stiff compared to the flapwise one, and, the corresponding loads are driven just by the gravity. In fig. 7, the blade tip extension is presented. The linear model predicts a positive extension due to the centrifugal force, while, the three non-linear models consistently predict the virtual axial shortening of the blade due to the bending.

Regarding the loads, the non-linear models predict considerably higher amplitude of the blade root torsion moment due to the bending-torsion coupling, as seen in fig. 8. The linear model results to an almost constant torsion moment, independent of the azimuth position of the blade. Its mean value is reduced about 40% compared to all the non-linear beam models, which predict almost the same mean values of the torsion moment. The amplitude of the variation is identical for the non-linear DC and non-linear EB models, while, the non-linear SB model predicts reduced amplitude ($\sim 30\%$).

In similar with the flapwise deflections (fig. 5), the amplitude of the flapwise bending moment at the blade root (fig. 9) is clearly affected by the increase in the amplitude of the twist angle (fig. 4). This is depicted in the results of all the non-linear models. Specifically, the non-linear DC model predicts a slightly increased amplitude of the variation ($\sim 5\%$) compared to the non-linear EB model, while, the other models follow with $\sim 20\%$ reduced amplitude for the non-linear SB model and $\sim 70\%$ reduced amplitude for the linear one, compared to the non-linear DC model. The mean value of the flapwise moment is almost the same for the non-linear DC, the non-linear EB and the linear model, while, the non-linear SB model predicts slightly increased mean value. A good agreement between the three non-linear models is obtained in the phase of the signal (which again follows the phase of the twist angle variation).

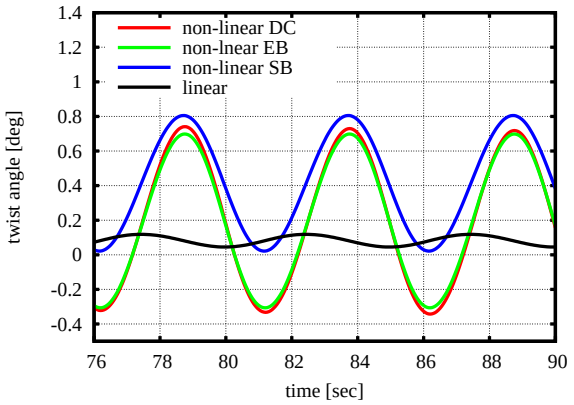

Fig. 4: Time history of the tip twist angle.

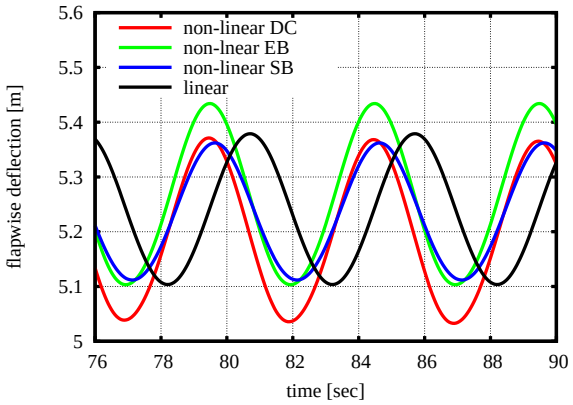

Fig. 5: Time history of the tip flapwise displacement.

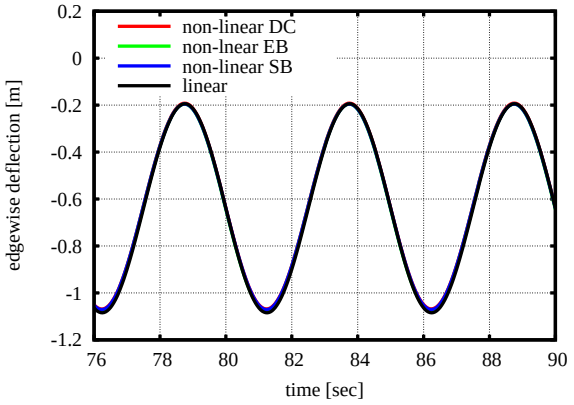

Fig. 6: Time history of the tip edgewise displacement.

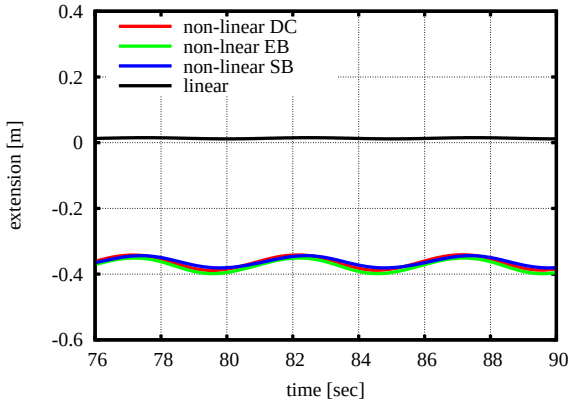

Fig. 7: Time history of the tip extension.

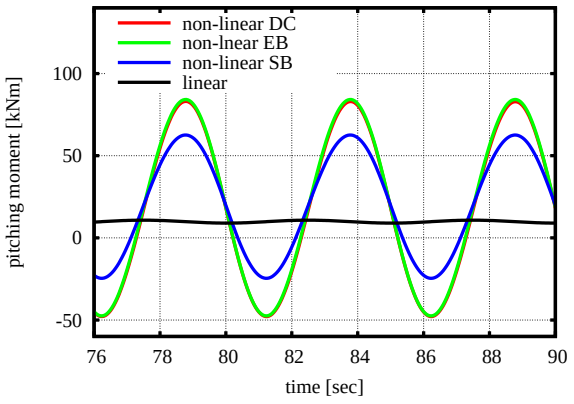

Fig. 8: Time history of the root pitching moment.

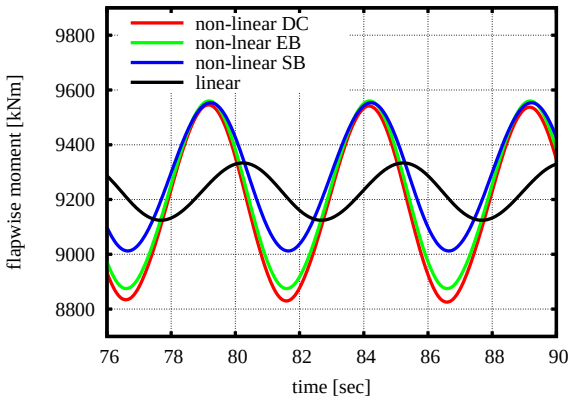

Fig. 9: Time history of the root flapwise bending moment

5 CONCLUDING REMARKS

A Total Lagrangian degenerate-continuum based Timoshenko beam approach was presented. The important features are that there is no constraint in the magnitude of displacements and rotations and that the beam model may be easily extended to a general curved beam. The main kinematic assumption is that the cross-sectional plane remains planar and rigid during deformation, although warping can be included in the formulation.

The present beam approach was implemented in the multi-body hydro-servo-aeroelastic tool hGAST. The stiffness of the beam is derived by retaining all the geometrical non-linear terms from the Green strain tensor, while, the beam inertia is taken into account using the initial configuration. The aeroelastic analysis of the three-bladed rotor of the 5MW NREL reference wind turbine was performed. The numerical results compare four modelings, the present beam approach, the 2nd order Euler-Bernoulli, the sub-body and the linear one, to assure the validity of the present formulation. The comparisons show that the present formulation works well, while the non-linear coupling effects compare well with the 2nd order Euler-Bernoulli beam theory model. The basic outcome from the analyses is that the geometrical non-linearity is significant w.r.t. the torsion-bending coupling terms and this is shown mainly in the torsional response, which is the basic factor for the determination of the aerodynamic loading.

ACKNOWLEDGMENT

The first author wishes to acknowledge the funding received towards the present work from the Fanourakis Foundation fellowship and Leventis Foundation fellowship. She also wishes to thank MSc. Structural Engineer Evangelos Katsavrias for his support in programming and for helpful discussions.

REFERENCES

[1] V. Riziotis, S. Voutsinas, GAST: A general aerodynamic and structural prediction tool for wind turbines, *EWEC Conference*, Dublin Castle, Ireland, 1997.

[2] D. Manolas, Hydro-aero-elastic analysis of offshore wind turbines, *PhD Thesis*, NTUA, Athens, 2015.

[3] M. A. Crisfield, *Non-linear finite element analysis of solids and structures, Vol. 2: Advanced topics*. John Wiley & Sons Ltd., 1997.

[4] K-J. Bathe, *Finite Element Procedures*. Prentice-Hall, Inc., 1996.

[5] E. N. Dvorkin, E. Oñate, J. Oliver, On a non-linear formulation for curved Timoshenko beam elements considering large displacement/rotation increments, *International Journal for Numerical Methods in Engineering*, **26**, 1597-1613, 1988.

[6] E. Reissner, On one-dimensional finite-strain beam theory: the plane problem, *Journal of applied mathematics and physics (ZAMP)*, **23**, 795-804, 1972.

[7] J. C. Simo, A finite strain beam formulation. The three-dimensional dynamic problem. Part I, *Computer Methods in Applied Mechanics and Engineering*, **49**, 55-70, 1985.

[8] S. Ahmad, B. M. Irons, O. C. Zienkiewicz, Curved thick shell and membrane elements with particular reference to axi-symmetric problems, *Proc. 2nd Conf. Matrix Methods in Structural Mechanics.* Wright-Patterson Air Force Base, Ohio, 1968.

[9] E. Reissner, On finite deformations of space-curved beams, *Journal of applied mathematics and physics (ZAMP)*, **32**, 734-744, 1981.

[10] G. Jelenić, M. A. Crisfield, Geometrically exact 3D beam theory: implementation of a strain-invariant finite element for statics and dynamics, *Computer Methods in Applied Mechanics and Engineering*, **171**, 141-171, 1999.

[11] A. Cardona, M. Geradin, A beam finite element non-linear theory with finite rotations. *International Journal for Numerical Methods in Engineering*, **26**, 2403-2438, 1988.

[12] A. Ibrahimbegocić, On finite element implementation of geometrically nonlinear Reissner's beam theory: three-dimensional curved beam elements, *Computer Methods in Applied Mechanics and Engineering*, **122**, 11-26, 1995.

[13] P. Zhang, S. Huang, Review of aeroelasticity for wind turbine: Current status, research focus and future perspectives, *Frontiers in Energy*, **5(4)**, 419-434, 2011.

[14] D. H. Hodges, E. H. Dowell, Nonlinear equations of motion for the elastic bending and torsion of twisted nonuniform rotor blades, *NASA TN D-7818*, 1974.

[15] D. H. Hodges, *Nonlinear Composite Beam Theory, Volume 213 Progress in Astronautics and Aeronautics*. American Institute of Aeronautics and Astronautics Inc., 2006.

[16] P. F. Pai, *Highly Flexible Structures: Modeling, Computation, and Experimentation*. American Institute of Aeronautics and Astronautics Inc., 2007.

[17] S. G. Voutsinas, V. A. Riziotis, P. Chaviaropoulos, Non-linear aerodynamics and fatigue loading on wind turbines operating at extreme sites, *AIAA Paper* No. 97-0935, 1997.

[18] Z. Q. Chen, T. J. A. Agar, Geometric nonlinear analysis of flexible spatial beam structures, *Computers & Structures*, **49(6)**, 1083-1094, 1993.

[19] H. Goldstein, C. Poole, J. Safko, *Classical mechanics*. Third edition, Addison Wesley, 2001.

[20] J. Jonkman, S. Butterfield, W. Musial, G. Scott, Definition of a 5-MW Reference Wind Turbine for Offshore System Development. *Technical Report, NREL/TP-500-38060*, February 2009.

[21] J. Argyris, An excursion into large rotations. *Computer Methods in Applied Mechanics and Engineering*, **32**, 85-155, 1982.

[22] J. C. Simo, L. Vu-Quoc, A three-dimensional finite-strain rod model. Part II: Computational aspects, *Computer Methods in Applied Mechanics and Engineering*, **58**, 79-116, 1986.

[23] M. Papadrakakis, *Analysis of Structures with the Finite Element Method (in Greek)*, Papasotiriou Publics, 2001.

[24] C. J. Houbolt, W. G. Brooks, Differential equations of motion for combined flapwise bending, chordwise bending, and torsion of twisted nonuniform rotor blades, *NACA Technical Note 3905*, 1958.

[25] M. Ritto-Corrêa, D. Camotim, On the differentiation of the Rodrigues formula and its significance for the vector-like parameterization of Reissner-Simo beam theory, *International Journal for Numerical Methods in Engineering*, **55**, 1005-1032, 2002.

[26] A. Ibrahimbegović, F. Frey, I. Kožar, Computational aspects of vector-like parametrization of three-dimensional finite rotations, *International Journal for Numerical Methods in Engineering*, **38**, 3653-3673, 1995.

[27] J. C. Simo, L. Vu-Quoc, On the dynamics in space of rods undergoing large motions - A geometrically exact approach, *Computer Methods in Applied Mechanics and Engineering*, **66**, 125-161, 1988.

[28] D. I. Manolas, V. A. Riziotis, S. G. Voutsinas, Assessing the importance of geometric nonlinear effects in the prediction of wind turbine blade loads, *Journal of Computational and Nonlinear Dynamics*, **20(4)**, ASME, 2015.